CrossMark

TECHNICAL PAPER

Scaling and super-cooling in heat storage harvesting devices

M. E. Kiziroglou[1,4] · A. Elefsiniotis[2] · N. Kokorakis[2] · S. W. Wright[1] · T. T. Toh[1] ·
P. D. Mitcheson[1] · U. Schmid[3] · Th. Becker[2] · E. M. Yeatman[1]

Abstract Aircraft sensors are typically cable powered, imposing a significant weight overhead. The exploitation of temperature variations during flight by a phase change material (PCM) based heat storage thermoelectric energy harvester, as an alternative power source in aeronautical applications, has recently been flight tested. In this work, the applicability of this technology to use cases with smaller and larger size specifications is studied by fabrication, testing and analysis of a scaled-down and a scaled-up prototype. Output energy of 4.1 J/g of PCM from a typical flight cycle is demonstrated for the scaled-down device, and 2.3 J/g of PCM for the scaled-up device. The higher energy density of the scaled down prototypes is attributed to the reduction in temperature inhomogeneity inside the PCM. The impact of super-cooling on performance is analyzed by employing a simulation model extended to include super-cooling effects. It is found that super-cooling may be beneficial for scaling down, in applications with slow temperature fluctuations.

✉ M. E. Kiziroglou
m.kiziroglou@imperial.ac.uk

1   Department of Electrical and Electronic Engineering,
    Imperial College London, London SW7 2AZ, UK

2   Communication and Sensor Department, Airbus Group
    Innovations, 81663 Munich, Germany

3   Institute of Sensor and Actuator Systems, Vienna University
    of Technology, 1040, Wien, Austria

4   Department of Automation Engineering, Alexander
    Technological Educational Institute of Thessaloniki, 57400,
    Thessaloniki, Greece

1 Introduction

Energy harvesting as the technology of collecting environmental energy that is locally available to power microsystems such as sensors was proposed at the beginning of the 2000 s (Glynne-Jones et al. 2004; Mitcheson et al. 2004; Shenck and Paradiso 2001; Sodano et al. 2005). Fifteen years on, a wealth of different approaches and device implementations have been proposed for exploiting motion, heat gradients, RF radiation and light sources. The exploitation of such approaches in useful applications requires that the net available power density is high enough, and that it is available at the desired location, for the desired period of time. In thermoelectric energy harvesting, this translates to the requirement for a temperature difference ΔT at the location of installation. Temperature differences are prevalent in industrial environments or in operating engines but they do not necessarily always occur at the required location. This has been a critical limitation in the application of thermoelectric harvesting devices.

For the case of environments where the temperature fluctuates considerably with time, a dynamic thermoelectric harvesting approach has been proposed, using a heat storage unit containing a phase change material (PCM) to induce temperature hysteresis, thereby creating an artificially increased ΔT internal to the device compared to an approach applying a sensible heat storage material. Based on this approach, various prototypes have been reported and the operation and performance of such devices has been analysed (Kiziroglou et al. 2014). For aircraft monitoring applications, where a considerable temperature cycle occurs during flight, tests have been performed for the characterisation of power generation performance (Elefsiniotis et al. 2013), and another flight test is planned for the demonstration of energy harvester-powered wireless strain

🖄 Springer

monitoring (Toh et al. 2014). The use of dynamic thermo-electric harvesting has also been considered in countryside environments for applications such as precision agriculture (Papachristou et al. 2013).

The typical volume of the PCM used in prototypes reported so far is in a range of around 20 cm^3. In order to assess the applicability of such devices to different sensor types or application scenarios, it would be useful to know how the performance of these devices scales with size. Therefore, in this work, two new heat storage thermoelectric harvesting devices are presented: one smaller and one larger than the typical size of devices already reported in the literature. The change of PCM volume is approximately an order of magnitude for both. In this way, a first assessment of scalability of this device concept is obtained.

In the following sections, the concept of dynamic thermoelectric harvesting is briefly summarized and then the scaled down and the scaled up prototypes are presented. The results are analyzed by comparison with simulation results obtained using a previously developed numerical model, extended here to account for super-cooling effects. The results are discussed and compared with previously reported devices. Finally, a functional demonstrator, a microcontroller operating while directly powered from the heat storage harvester using a voltage booster and regulator is presented, and conclusions are drawn about the potential use of dynamic thermoelectric harvesting in commercial applications.

2 Device concept

The principle of operation of heat storage thermoelectric harvesting devices has been discussed in detail in previous
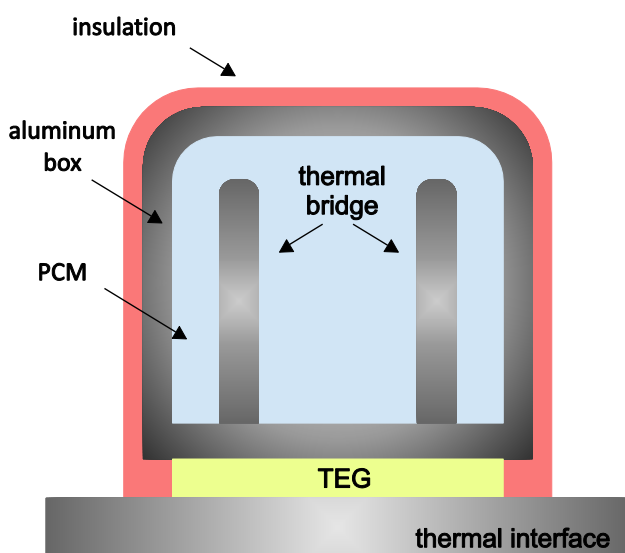

Fig. 1 Internal structure of phase change thermal harvesters

publications (Becker et al. 2015; Kiziroglou et al. 2014). For easy reference, the concept is summarized here, with reference to Fig. 1. The device objective is to transform thermal energy from the temperature fluctuation of an environment into electrical energy. A high heat capacity heat storage unit (HSU) is employed, containing a PCM that changes phase within the operating temperature range, thereby increasing the induced heat flow. The HSU is in thermal contact with the environment only through a thermoelectric generator (TEG). As the environmental temperature fluctuates, heat flows in and out of the HSU through the TEG, resulting in generation of electrical power. The high heat capacity of the HSU and, critically, the phase change (i.e. latent) heat of the PCM ensures that a considerable ΔT is built up across the TEG.

The temperature and phase change uniformity inside the HSU can be enhanced by metal thermal bridging, such that any ΔT loss across the PCM is minimized. The overall power output of such devices scales with ΔT^2, because both the heat flow and the TEG efficiency scale approximately linearly with ΔT. In voltage terms, this is equivalent to saying that the voltage output of a TEG is proportional to ΔT and hence output power scales with ΔT^2. An analysis of the dynamics of operation and performance of this type of device has been presented in (Kiziroglou et al. 2014) and (Kiziroglou et al. 2013).

3 Efficiency for maximum power

A summary of efficiency considerations that are important particularly for heat storage energy harvesting devices is presented in this section. If T_h, T_c and $T = (T_h + T_c)/2$ are respectively the hot side, cold side and average TEG temperatures, the efficiency as a function of the ratio μ of load resistance R_L over the internal electrical resistance of the TEG, R_e can be written as:

$$\eta_{TEG} = \frac{\Delta T}{T_h} \cdot \frac{\mu}{\frac{(1+\mu)^2}{ZT_h} + (1+\mu) - \frac{\Delta T}{2T_h}} \tag{1}$$

The maximum efficiency occurs when R_L is such that $\mu = \sqrt{1 + ZT}$, giving:

$$\eta_{TEG,max} = \frac{\Delta T}{T_h} \cdot \frac{\sqrt{1 + ZT} - 1}{\sqrt{1 + ZT} + \frac{T_c}{T_h}} \tag{2}$$

where $ZT = a^2T/(R_eK)$ is the TEG figure of merit, a its Seebeck coefficient and K its heat conductance. This operation point is different from the maximum output power point, which occurs for $\mu = 1$, giving:

$$\eta_{TEG,Pmax} = \frac{\Delta T}{T_h} \cdot \frac{1}{2 + \frac{4}{ZT_h} - \frac{\Delta T}{2T_h}} \tag{3}$$

The difference originates from the influence of the Seebeck and ohmic effects on the heat flow, represented by the second and third terms in the denominator of Eq. (1). These effects result in lower heat flow for a given ΔT. In other words, the return of the electrical power back to heat through these effects, results in an increase of the actual thermal resistance of a TEG and in a difference between the points of maximum conversion efficiency and maximum power delivery. In conventional TEG applications, the output power is often more important. In contrast, in heat storage thermoelectric harvesting efficiency plays a more significant role, because the total available heat is limited. The optimal electrical load for maximum cumulative energy therefore depends on the heat storage dynamics, especially if the transduction efficiency is high enough for a significant heat flow modulation. A comprehensive analysis of this effect would need to include the heat leakage of the HSU. Overall, this shift of the optimal operation point may allow an increase of performance and should be taken into account in the design and implementation of heat-storage based power supplies. A more detailed analysis of thermoelectric conversion efficiency can be found in chapters 4, 6 and 20 of (Briand et al. 2015).

In the evaluation of the devices that are presented in this paper, the maximum power delivery operation point was used, because for the relevant ZT values and ΔT range, the corresponding efficiency difference is less than 6 %, and the gain in cumulative energy output is expected to be reduced by heat leakage from the HSU to the environment.

4 Numerical modeling including super cooling

A numerical model for heat storage thermoelectric harvesting devices has been introduced in (Kiziroglou et al. 2014), and extended to include temperature inhomogeneity effects in the PCM in (Kiziroglou et al. 2013). According to this model, which includes temperature inhomogeneity in the PCM, a numerical simulation of the system dynamics is possible by calculating every new state $(T_{in}(n + 1), \dot{Q}(n + 1))$ from the previous $(T_{in}(n), \dot{Q}(n))$ and a given T_{out} profile, for a time step Δt, using the following equations:

$$T_{in}(n+1) = \begin{cases} T_{in}(n) + (T_{out}(n) - T_{in}(n)) \cdot \frac{\Delta t}{RC} \ (nonphasechange) \\ T_{in}(n) + \frac{(T_{out} - T_{in})^2}{R^2 k \rho L A^2} \Delta t \ (phasechange) \end{cases}$$

$$\dot{Q}(n+1) = \dot{Q}(n) + (T_{out}(n) - T_{in}(n)) \cdot \frac{\Delta t}{RC} \tag{4}$$

In these equations R and C are the thermal resistance between the HSU and the environment, and the thermal

capacity of the HSU respectively. The parameters k, ρ and L are the heat conductivity, density and latent heat of the PCM respectively. The parameter A is the surface area of the TEG heat sink in the HSU. The electrical power and cumulative energy output can then be calculated by:

$$P(n) = \eta_{TEG}(n) \cdot \dot{Q}(n)$$
$$E(n) = \sum_{n=1}^{n=max} P(n) \cdot \Delta t \tag{5}$$

The efficiency η_{TEG} can be calculated from (2), if the ZT of the TEG used in known. A more direct way to calculate the electrical power is through the Seebeck coefficient of the device. If a and R_i are known, then the maximum output power will be provided on a matched load $R_L = R_e$ (i.e. $\mu = 1$), at a value of:

$$P = \frac{V^2}{4R_e} = \frac{a^2 \Delta T^2}{4R_e} \tag{6}$$

and, for the numerical model:

$$P(n) = \frac{a^2}{4R_e}(T_{out}(n) - T_{in}(n))^2 \tag{7}$$

In practise, the latter method can be more accurate, because the effective Seebeck coefficient of a particular device can be determined directly by a linear fit of experimental $V - \Delta T$ measurements. This method will be used in the analysis of the experimental results presented in Sects. 5 and 6.

In previous implementations, the switching between phase change and non-phase-change operation was done by comparing T_{in} to the phase change temperature T_{PC}. When T_{PC} is reached, the model enters its phase change mode, until the PCM latent heat is exhausted. For the work presented here, an extension of this model was developed, to account for super-cooling effects. This extension allows the specification of a super-cooling temperature level T_{SC}, which needs to be reached before phase change occurs. This additional level applies only during a cooling-down stage. When the super-cooling level is reached, phase change is triggered and the PCM changes abruptly its temperature to the phase change temperature. Then, the non-homogeneous phase change begins, but with a smaller-than-normal remaining latent heat. This difference is equal to the amount of sensible heat that was released during super-cooling. Physically, this reflects the effect that the transition from a super-cooling condition to the phase change temperature T_{PC} is accompanied by energy transfer from a latent to a sensible form, such that the liquid can increase its temperature to T_{PC}. The amount of this energy is $(T_{PC} - T_{SC}) \cdot C$, where C is the heat capacity of the PCM in liquid form.

5 Scaled down prototype

The size of previously reported heat storage harvesting prototypes is around 100 cm^3, with a PCM material volume in the range of 10–30 cm^3. In this section, a scaled-down prototype is presented, based on two different TEG models. The first is the Marlow NL1013T 13 × 13 × 2.4 mm TEG, with an internal electrical resistance of 7.42 Ω and a thermal resistance of 16.9 K/W. This corresponds to a thermal conductivity of 0.68 W/m K. The second is the Eureca TEG1-9.1-9.9-0.8/200 with size 9.1 × 9.9 × 2.3 mm, internal electrical resistance 8.85 Ω and thermal resistance 30 K/W. This corresponds to a thermal conductivity of 0.85 W/m K. The specifications of the TEGs used are summarised in Table 1.

The heat storage unit comprises an extruded polystyrene (XPS) lid-less box with outer dimensions 19 × 19 × 27 mm and inner dimensions 10 × 10 × 19 mm and a 9-fin 14 × 14 × 20 mm aluminum thermal bridge. The total HSU capacity, taking into account the thermal bridge displacement, is 1.8 ml. For the experiments, 1.4 ml of water was used as the PCM. A photograph of the device, with the Marlow TEG installed, is shown in Fig. 2 (left). The thermal bridge is protruding from the box for illustrative purposes. In Fig. 2 (right), a photograph of the device under characterization is shown, featuring the insulated TEG and Pt100 sensor connectors.

The device was characterized in an environmental chamber for various different temperature cycles and with the aircraft environment as an indicative application case. The temperature profiles used were based on previously reported data for an aircraft fuselage during flight (Elefsiniotis et al. 2013). The TEG output voltage was monitored across a connected 7.5 Ω matched load. It is noted here that, as has been demonstrated in (Kiziroglou et al. 2014) and summarized in Sect. 3, the optimal load for maximum power is not the same as for maximum efficiency. In the experiments presented in this paper, the devices were tested under maximum power (i.e. matched load) conditions, for simplicity.

The temperature response of the scaled-down prototype with the Marlow TEG installed is presented in Fig. 3. The environmental and the HSU temperature are denoted as T_{out} and T_{in} respectively. The T_{out} cycle was from +22 to −25 °C and back, with a temperature change rate of approximately 3 °C/min, similar to that observed during typical flight scenarios. A ΔT as high as 15 °C is achieved during the cooling down phase, with significant water

Table 1 Summary of specifications for the TEGs used in the two scaled-down and the scaled-up prototypes

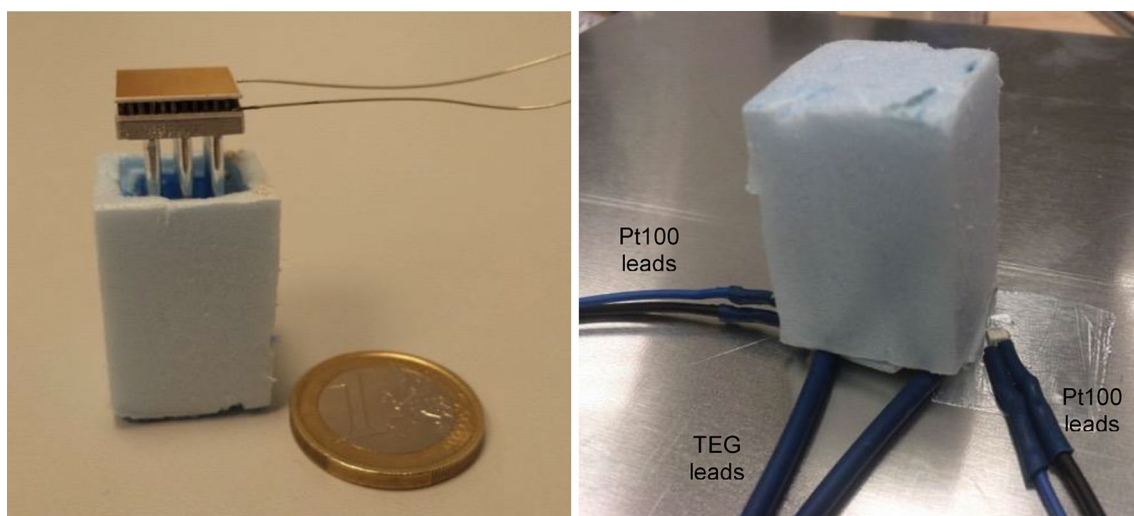| Manufacturer	Model	Dimensions (mm)	Internal electrical resistance (Ω)	Thermal resistance (K/W)	Thermal conductivity (W/(m K))
Marlow	NL1013T	13.2 × 13.2 × 2.4	7.42	16.4	0.85
Eureca	TEG1-9.1-9.9-0.8/200	9.1 × 9.9 × 2.3	8.85	30	0.85
Marlow	TG12-6L	40.1 × 40.1 × 3.9	3.8	1.58	1.54

Fig. 2 Images of the scaled down prototype. *Left* open device exhibiting the extruded polystyrene (XPS) heat storage unit, the internal heat sink and the TEG. *Right* device under test
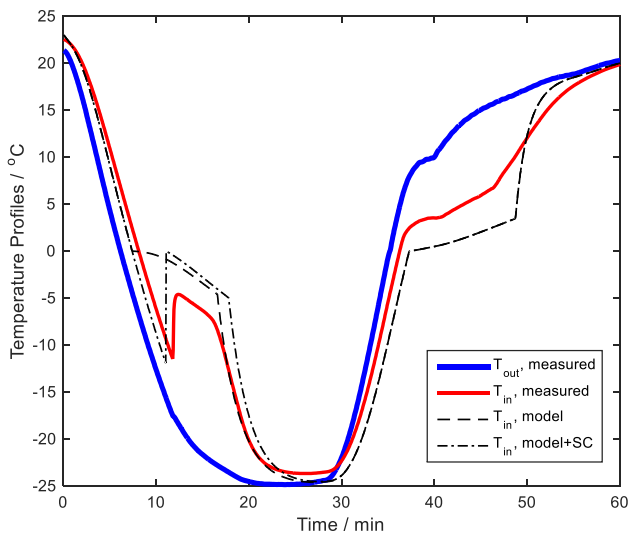
Fig. 3 Temperature response of the scaled-down prototype (1.4 ml of PCM) during a typical flight temperature cycle using the Marlow TEG. The environmental and HSU temperatures are denoted as T_{out} and T_{in} respectively. Corresponding model responses using the inhomogeneous phase change model with and without super-cooling (SC) are also shown

super-cooling. During the warm up phase, the ΔT is substantially smaller, mainly due to the slower change of temperature that can be achieved by the environmental chamber. This is due to the large heat absorption from the HSU that occurs during phase change. The large temperature difference that is created results in a high heat flux which disrupts the temperature uniformity in the environmental chamber. In turn, this delays the response of the temperature control system, leading to a slower and distorted T_{out} profile during warm-up that is observed between minutes 35 and 45 in Fig. 3. Such effects do not occur in a flight environment, because there, the heat sink of the HSU is the fuselage of the aircraft, with a practically unlimited heat capacity. This means that in an applied environment, and provided that a good thermal contact is achieved by the installation method used, the T_{out} profile experienced by the harvesting device is not affected by the operation of the device itself.

The temperature response of the device was also simulated, using the model presented in Sect. 3. The results are shown as a dashed curve in Fig. 3, using as-measured parameter values. In particular, for the HSU thermal resistance R, the nominal value of the TEG thermal resistance (16.4 K/W) was used. Heat leakage through the polystyrene insulation was not taken into account. For the HSU heat capacity C, both the sensible heat of the PCM and that of the aluminium heat bridge were taken into account. For water, a specific heat capacity of 4.2 kJ/kg K in liquid form and 2 kJ/kg K in solid form was assumed, and a latent heat

of L = 334 kJ/kg (Kiziroglou et al. 2013). For aluminium, a heat capacity of 0.9 kJ/kg K was assumed. The device response to the experimentally measured T_{out} cycle can then be simulated, accounting for the 1.4 g of water, the aluminium heat bridge mass which was measured to be 1.72 g, the PCM-Al interface surface of 684 mm^2 and taking the nominal heat conductivity value for water, 0.58 W/m K as the effective conductivity during phase change. Parametric fitting was avoided to maintain simplicity in the interpretation of the comparison.

The simulation curve follows the different effects that are captured by the measured data, and shows good matching in the exponential cooling down stage gradient, in the inhomogeneous phase change temperature gradient and the phase change duration. The simulation model used for the dashed curve on Fig. 3 does not include super-cooling. The introduction of super-cooling to the model is possible. Such a simulation is shown as a dash-dotted line in Fig. 3. This effect and its importance to the performance of heat storage thermoelectric harvesting device will be discussed in Sect. 5.

The corresponding TEG output voltage, measured using a data logging multimeter across a 7.5 Ω load, and the corresponding cumulative energy, calculated directly as $E = \int V^2/R_L dt$ are presented in Fig. 4. The total cumulative energy harvested from a full temperature cycle was 5.8 J. This corresponds to an energy density of 4.14 J/g of PCM, around 10 % lower than the corresponding 4.57 J/g that has been previously reported for a device with 23 g of PCM. The electrical power and energy output that correspond to the simulated device response can be calculated
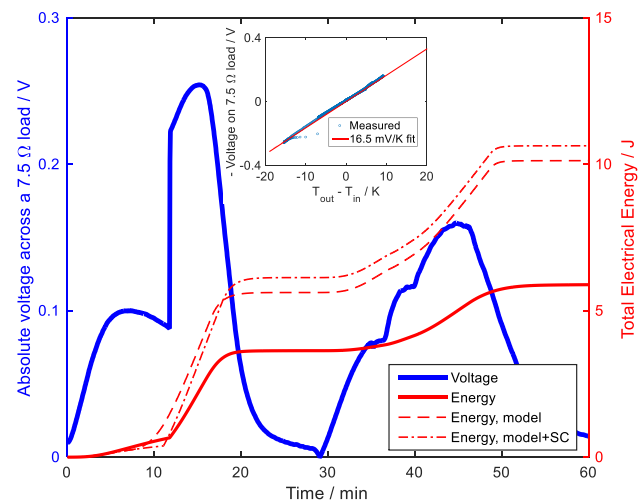

Fig. 4 Voltage and energy output, on a 7.5 Ω load, of the scaled-down prototype corresponding to the temperature cycle of Fig. 3. The corresponding modeled energy performance is also plotted, using an effective Seebeck coefficient of 16.5 mV/K which was determined from fitting the V − ΔT measurements as shown in the *inset*

either from the heat power flow, using the TEG efficiency equation at optimum load operation, or through the determination of an effective Seebeck coefficient for the HSU-TEG system, which can be found by a linear fit of the measured voltage-ΔT data. Such a fit for the device under study is shown in the inset of Fig. 4. A TEG output of 16.5 mV/K is found across a 7.5 Ω load. As this load value matches the internal resistance of the TEG, the corresponding open-circuit voltage is twice the closed-circuit one. Hence, the effective Seebeck coefficient of the device is 33 mV/K. The corresponding simulated energy curves, for the model without and with super-cooling, are shown as a dashed and a dash-dot curve in Fig. 4 respectively. These curves both predict a higher output energy for this device. This deviation can be attributed to temperature inhomogeneity which creates a lag between the temperature in the PCM bulk and the temperature at the sensor location, which shows phase change at around -5 °C at cool-down, and around $+2$ °C during warm up. This error in the temperature measurements leads to an over-estimation of the effective Seebeck coefficient from the V $- \Delta T$ fit, and in turn, to the cumulative energy being over-estimated.

Similar results are obtained using the Eureca TEG, connected to a matched 8.8 Ω load. The temperature response of this device to a flight temperature cycle is shown as a light (red in the online version) curve in Fig. 5. The experimental results are again compared with a simulation of device performance, using a numerical model which includes a non-homogeneous phase change approximation, with and without super cooling. All parameters were the same as with the simulation run of Fig. 3, except for
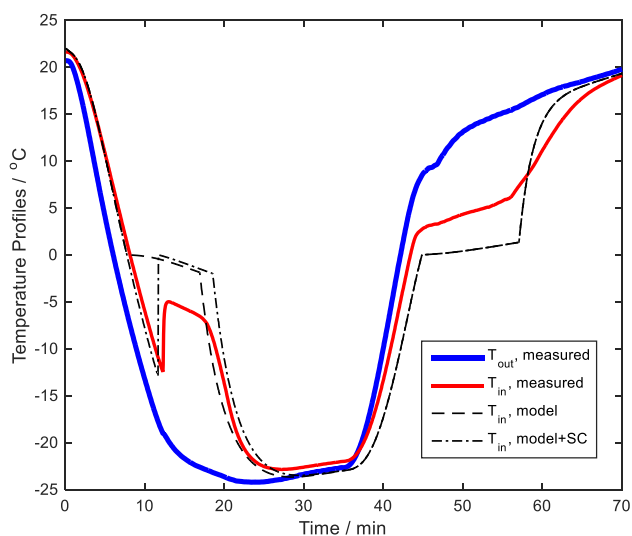

Fig. 5 Temperature response of the scaled-down prototype during a typical flight temperature cycle using the Eureca TEG. The corresponding model responses are also shown for comparison, with a fitted PCM volume value of 0.9 $\pm$ 0.1 cm^3
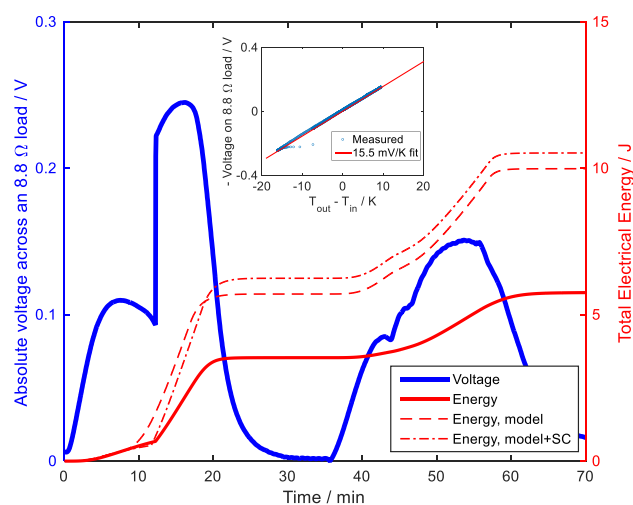
Fig. 6 Voltage and energy output on an 8.8 Ω load of the scaled-down prototype, with the Eureca TEG, corresponding to the temperature cycle of Fig. 5. The V $- \Delta T$ fit is shown in the *inset*. The modeled energy performance is also plotted for comparison

the TEG heat resistance which was set to the nominal value given by the Eureca TEG specifications (i.e. 30 K/W), and for the PCM volume which was determined, by fitting of the simulation to the experimental phase change duration, to be 0.9 $\pm$ 0.1 ml. The corresponding curves are shown as a dashed and a dash-dot curve in Fig. 5 respectively. Better matching in the exponential (non-phase change) regions is obtained, and similar matching in the phase-change gradient. The deviation of phase change temperature is again apparent.

The voltage response, measured across an 8.8 Ω resistive load, and the corresponding cumulative harvested energy are illustrated in Fig. 6. The total cumulative energy from a full temperature cycle was 5.5 J, corresponding to an energy density of 3.93 J/g of PCM for this implementation. As before, the electrical power and energy output can be simulated, using the simulated T_{in} profile and calculating the output voltage through the effective Seebeck coefficient of the system, which can be determined by fitting the measured V $- \Delta T$ data as shown in the inset of Fig. 6. A value of 15.5 mV/K is obtained, slightly less than that of the same HSU with the Marlow TEG. As before, both models overestimate the cumulative energy because the transient-induced offset error of the temperature measurements leads to an overestimation of the effective Seebeck coefficient.

6 Scaled up prototype

For the scaled up prototype, a 40.1 $\times$ 40.1 $\times$ 3.9 mm Marlow TG12-6L TEG model was used, with an internal electrical resistance of 3.8 Ω and a thermal resistance of 1.58 K/W.

This corresponds to a thermal conductivity of 1.54 W/mK. Again, the reference to the value of thermal conductivity, in addition to the thermal resistance, for the TEG is given for a model-independent comparison of available technologies.

The heat storage unit comprises an extruded polystyrene lid-less box with outer dimensions 74 × 135 × 42 mm and inner dimensions 48 × 108 × 34 mm and a size matching multi-fin aluminum thermal bridge. The total HSU volume capacity, taking into account the thermal bridge displacement, is 140 cm^3. For the experiments, 110 cm^3 of water were used as PCM allowing substantial space for expansion during temperature sweep and phase change, which is expected to be at around 10 % of the volume within the range used during experiments. As with the scaled down prototype, the device was characterized in an environmental chamber for various different temperature cycles. The TEG output was connected to a matched 3.8 Ω load.

The temperature response of the scaled-up prototype is presented in Fig. 7. The cycle was from +22 to −20 °C and back, with a temperature change rate of around 4 K/min, similar to the ones presented for the scaled down prototype. The impact of the device heat absorption and release to the performance of the environmental chamber is more pronounced, temporarily disrupting the applied temperature cycle. This effect leads to underestimation of the device performance in a real environment. A ΔT of 15 °C is achieved both during the cooling down and the warming up phases.

In order to simulate the response of the scaled-up prototype, a new set of parameters is required, to reflect the different heat bridge, TEG and amount of PCM used, in comparison with the devices of the previous section. As before,
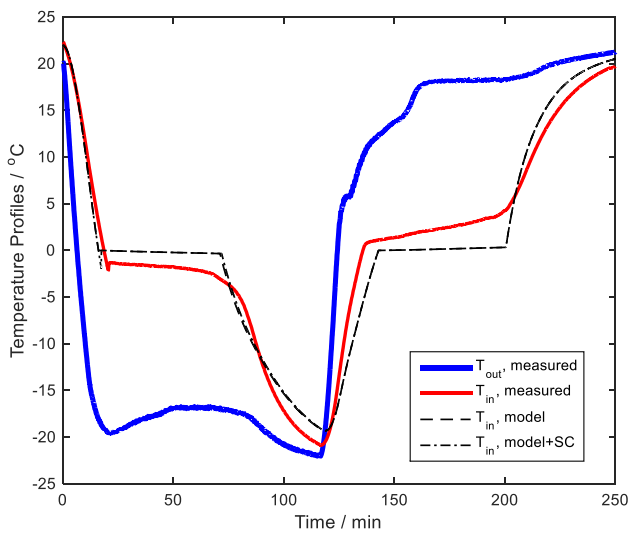
for the HSU thermal resistance R, the nominal value of the TEG thermal resistance (1.58 K/W) was used, neglecting heat leakage through the insulation. The PCM and aluminium masses were 110 and 238 g respectively while the PCM-Al interface surface was 80 cm^2. The nominal values for water and aluminium properties were used, taking 0.58 W/m K as the effective conductivity during phase change. The non-fitted simulation curve matches well to the experimental data, with super-cooling being far less pronounced than in the case of the scaled-down devices. The phase change temperature shift is still present in the experimental data, although also substantially smaller (−1 and +1 °C at cool-down and warm-up respectively).

The corresponding voltage output, measured across a resistive load of 3.8 Ω, is shown as a bold (blue in online version) curve in Fig. 8. Using the same method as with the scaled-down prototypes, an effective Seebeck coefficient of 18.5 mV/K is found, as shown in the inset. The simulated cumulative energy curves are almost identical to each other and very close to the measured performance of the device. This is due to the very weak super-cooling that is observed (to be discussed in the following section) but also to the slower sweep of T_{IN} which occurs due to the significantly larger heat capacitance of the device. This slower temperature change reduces the temperature inhomogeneity in the device and, in turn, the deviation of the measured from the actual ΔT on the TEG. Hence, the Seebeck coefficient cumulative energy overestimation is much smaller than that of the smaller devices. The total experimentally measured energy harvested from a full temperature cycle was 254 J. This corresponds to an energy density of 2.31 J/g of PCM.
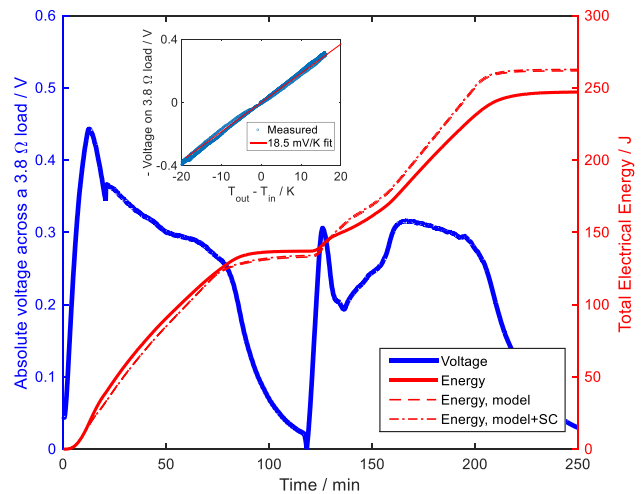

Fig. 7 Temperature response of the scaled-up prototype, with 110 ml of water as the PCM. Modeled responses are also shown for comparison. The model curves overlap due to weak super-cooling

Fig. 8 Voltage and energy output on a 3.8 Ω load of the scaled-up prototype, corresponding to the temperature cycle of Fig. 7. The corresponding modeled energy performance is also plotted for comparison, using the effective Seebeck coefficient value determined from the V − ΔT fit shown in the *inset*

7 Supercooling

From the performance analysis of the devices presented in this paper, and especially in the smaller devices, it is apparent that super cooling can have a significant effect on the output power of heat storage thermoelectric harvesting devices. Super-cooling causes a reduced ΔT during its occurrence. However, the reduced heat flow is preserved for the phase change stage, which usually maintains a higher ΔT and hence a more effective time for heat flow and conversion. This is due to the approximately linear dependence of TEG efficiency on the applied ΔT. Whether super-cooling has a positive or negative effect on the overall output energy depends on the environmental temperature change rate in comparison to the thermal time constant RC of the device (where R is the thermal resistance and C the thermal capacitance of the device). The RC values of the Marlow and Eureca TEG scaled-down devices and of the scaled-up device are 73 and 685 s for liquid state and 125 and 1067 s for solid state respectively. On the other hand, the 4 K/min temperature sweep rate applied in the experiments corresponds to a transition duration of 600 s. It is noted that the relative values of total available sensible and latent heat may also play a significant role in this effect.

The model presented in Sect. 4 was used to simulate the performance of the devices presented in this paper. The super-cooling temperature T_{PC} was set directly to the experimentally observed value. The difference in the temperature profiles is apparent in the case of the scaled-down devices (Figs. 3, 5), where super-cooling is pronounced. In terms of device performance, the comparison between simulation results of energy output with and without super-cooling can provide a useful indication. An example can be found in the comparison between the two simulation curves of Fig. 4.

During the super-cooling stage, the dash-dot (super-cooling included) curve provides less energy to the TEG, as a small ΔT is maintained. Hence, by the end of super-cooling (min 12 of the simulation) the TEG has delivered less energy than in the non-super-cooling case (dashed curve). However, during the phase change stage this is compensated by the release of reserved heat at a higher ΔT and hence higher efficiency, leading to an overall energy gain of around 5 %. The same gain is observed in Fig. 6 for the case of using the Eureca TEG.

As mentioned, no significant super-cooling was observed for the large scale prototype device. This could be attributed to the larger PCM mass, which makes the avoidance of solidification nucleation less likely. In order to draw a reliable conclusion about a correlation between super-cooling and device size, further investigation would be required, taking into account the effects of PCM purity, surface to volume ratio and surface texture but also the possibility of vibration-triggered nucleation.

8 State of the art of dynamic thermoelectric harvesters

A summary of the main features and energy density demonstrated by the three scaled devices presented in this paper is given in Table 2. For comparison, three other implementations of dynamic thermoelectric harvesting are also included. The performance of such devices depends significantly on the materials used and the design of the heat storage unit, including the thermal bridge and the insulation. Yet, all prototypes yield an energy density between 2.3 J and 5 J/g of PCM. The corresponding maximum theoretically achievable energy density for the particular

Table 2 Comparison of energy density among different dynamic harvester implementations using water as a PCM

| Organisation/year	Total device size (ml)	TEG	Energy J	Energy density (J/ml) (PCM)	Energy density (J/ml) (device)
EADS/2008 (Samson et al. 2010)	24 plus insulation	4 × Eureca TEG1-9.1-9.9-0.8/200	35	3.5	1.5 (without insulation)
LAAS-CNRS/2008 (Bailly et al. 2008)	–	Micropelt MPGD602	34	2.8	–
Imperial/2014 (Kiziroglou et al. 2014)	78	2 × Marlow TG12-2-5	105	4.57	1.3
Imperial and EADS/2015 (this paper, scaled-down 1)	9.7	Marlow NL1013T	5.8	4.14	0.6
Imperial and EADS/2015 (this paper, scaled-down 2)	9.7	Eureca TEG1-9.1-9.9-0.8/200	5.5	3.93	0.6
Imperial and EADS/2015 (this paper, scaled-up)	420	Marlow TG12-6L	254	2.31	0.6
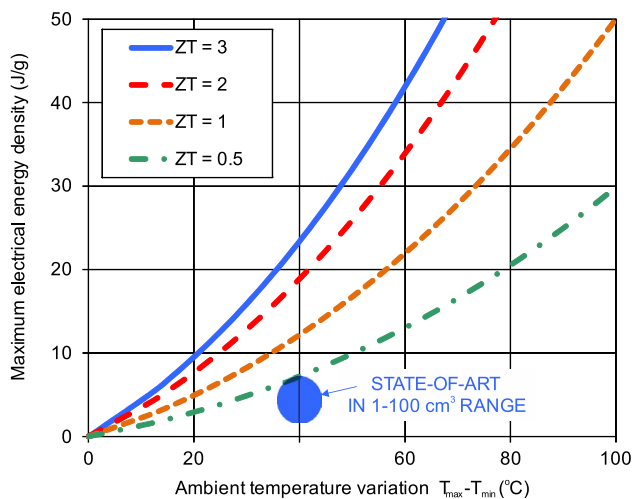
Fig. 9 State-of-the-art of performance for dynamic thermoelectric harvesting prototypes in comparison to the theoretical maximum electrical energy density for different TEG technologies

Fig. 10 Demonstrated electrical energy of recent dynamic thermoelectric harvesters as a function of PCM volume

temperature cycle used and the currently available TEGs (ZT ~ 0.7), is 10 J/g of PCM (Kiziroglou et al. 2014). The state-of-the-art of performance for dynamic thermoelectric harvesting prototypes is illustrated in Fig. 9, in comparison to the theoretical maximum electrical energy density for different TEG technologies.

The demonstrated electrical energy for all prototypes reported to date is plotted against PCM volume in Fig. 10. No increasing or decreasing trend can be identified for the energy density as a function of size. Nevertheless, smaller (or flatter) HSU designs in general may allow a smaller heat path and decreased temperature inhomogeneity in the PCM, meaning lower ΔT loss and higher conversion efficiency. It can be concluded that devices in the volume range 1–100 cm^3 can provide a useful amount of energy for their size. An instructive indication of power availability can be found in the comparison of performance, in terms of J per PCM volume, against state of the art non-rechargeable batteries. The 2.3–4.6 J/g output of the dynamic thermoelectric harvesting prototypes will reach the energy density of an alkaline battery (1.8 kJ/ml Energizer 2016) after 400–800 cycles of operation and a lithium one (2.4 kJ/ml Panasonic 2016) after 500–1000 cycles. Performance degradation is not expected due to the solid state nature of the TEGs and the chemically passive nature of the phase change materials used, contrary to chemical energy storage media like batteries.

With regard to the observation and discussion of the super-cooling effect, it is expected that applications with high temperature sweep rates would benefit from suppression of super cooling. In contrast, applications with low temperature sweep rates could benefit from (or, unde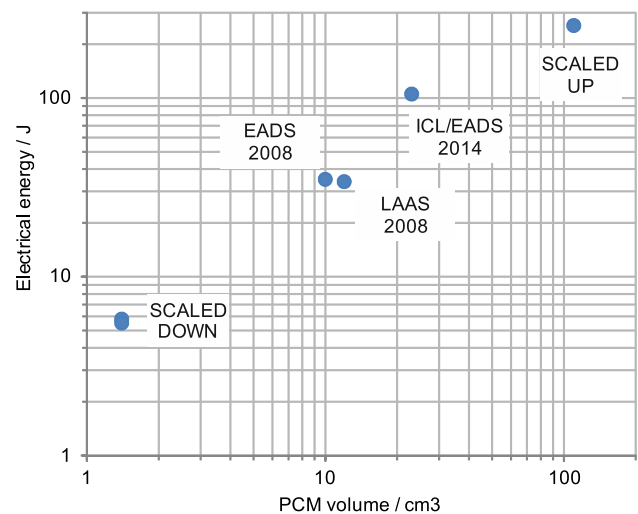r certain conditions, even rely on) super-cooling. In order to distinguish between the two cases, the thermal time constant RC, the PCM volume and the size of the device should be taken into account. Particularly, the indication that super-cooling in smaller devices could be both more likely and favourable is important for applications with small device sizes and slow temperature fluctuations.

Further studies on the scaling of dynamic thermoelectric harvesting devices could involve a combined multi-parameter analysis and numerical simulation. This could identify new methods and device designs, optimized for particular use cases.

References

Bailly N, Dilhac JM, Escriba C, Vanhecke C, Mauran N, Bafleur M (2008) Energy scavenging based on transient thermal gradients: application to structural health monitoring of aircrafts. In: 8th international workshop on micro and nanotechnology for power generation and energy conversion applications (PowerMEMS), Sendai, Japan, pp 205–208

Becker T, Elefsiniotis A, Kiziroglou ME (2015) Thermoelectric energy harvesting in aircraft. In: Briand D, Yeatman E, Roundy S (eds) Micro energy harvesting. Wiley, Weinheim, Germany. doi:10.1002/9783527672943.ch20

Briand D, Yeatman E, Roundy S (2015) Micro enegy harvesting. Wiley. doi:10.1002/9783527672943

Elefsiniotis A, Samson D, Becker T, Schmid U (2013) Investigation of the performance of thermoelectric energy harvesters under real flight conditions. J Electron Mater 42:2301–2305. doi:10.1007/s11664-012-2411-0

Energizer Holdings Inc. (2016) EN91 AA alkaline battery datasheet, Form No. EBC - 1202N. http://data.energizer.com/PDFs/EN91.pdf. Accessed 2 Mar 2016

Glynne-Jones P, Tudor MJ, Beeby SP, White NM (2004) An electromagnetic, vibration-powered generator for intelligent sensor systems. Sens Actuators A 110:344–349

Kiziroglou M, Elefsiniotis A, Wright S, Toh T, Mitcheson P, Becker T, Yeatman E (2013) Performance of phase change materials for heat storage thermoelectric harvesting. Appl Phys Lett 103:193902

Kiziroglou ME, Wright SW, Toh TT, Mitcheson PD, Becker T, Yeatman EM (2014) Design and fabrication of heat storage thermoelectric harvesting devices. Ind Electron IEEE Trans 61:302–309. doi:10.1109/tie.2013.2257140

Mitcheson PD, Green TC, Yeatman EM, Holmes AS (2004) Architectures for vibration-driven micropower generators. Microelectromech Syst J 13:429–440

Panasonic (2016) Coin type lithium batteries (CR series). Panasonic. http://industrial.panasonic.com/ww/products/batteries/primary-batteries/lithium-batteries/coin-type-lithium-batteries-cr-series. Accessed 09 Feb 2016 2016

Papachristou AA, Kiziroglou ME, Petrou L, Koundouras S, Hatzopoulos AA (2013) Viability of thermoelectric energy harvesting for precision agriculture sensor nodes. In: Paper presented at the 8th Jordanian International Electrical and Electronics Engineering Conference, Amman, Jordan, 16–18 Apr

Samson D, Otterpohl T, Kluge M, Schmid U, Becker T (2010) Aircraft-specific thermoelectric generator module. J Electron Mater 39:2092–2095. doi:10.1007/s11664-009-0997-7

Shenck NS, Paradiso JA (2001) Energy scavenging with shoe-mounted piezoelectrics. IEEE Micro 21:30–42

Sodano HA, Inman DJ, Park G (2005) Comparison of piezoelectric energy harvesting devices for recharging batteries. J Intell Mater Syst Struct 16:799–807. doi:10.1177/1045389x05056681

Toh TT, Wright SW, Kiziroglou ME, Mitcheson PD, Yeatman EM (2014) A dual polarity, cold-starting interface circuit for heat storage energy harvesters. Sens Actuators A 211:38–44. doi:10.1016/j.sna.2014.02.037